Problem Set 10 (**Due Nov. 18th**)

1. Discuss any upstream elements that are important for the initiation of transcription. Make sure to mention where these DNA sequences contact RNA Polymerase. These elements are only present upstream of select genes. What makes these genes particularly important/special?

2. In our discussion of the active sites of DNA Polymerase and RNA Polymerase, the elongation reaction was inhibited by the presence of very specific NTP adducts. For each enzyme, draw the structure of this molecule and identify exactly what is present or absent that inhibits chain elongation.

3. What is "abortive initiation" and why does it occur?

4. Explain the two ways that *E. coli* can terminate processive RNA polymerization.

5. Describe the mechanism RNA Polymerase uses form NTP sampling and processive elongation. Make sure to include the role of the Bridge and Trigger helices.

6. Describe how RecA and LexA work together to regulate the SOS response.

7. Describe the BER process. Make sure to include any cellular machinery that is important.

8. Investigate the structure of LexA bound to DNA (pdbID 3JSO). This protein binds to the DNA using a standard winged helix turn helix (wHTH) structural motif. Prepare and image with the wHTH motifs colored differently than the rest of the protein. What part of the B-form DNA does the recognition helix interact with. How about the wings?

9. Summarize the Excision Repair process. Use as much detail as you think appropriate.

10. UvrC contains 2 endonuclease domains. Each domain uses a divalent cation (typically Mg^{2+}) to promote catalysis. Propose a Mg^{2+} dependent mechanism for this reaction.

11. Using the attached paper about the structure of DnaB, answer the following questions. It may be useful to explore the pdb files associated with this paper.
    a. Define each acrynym: HBD, CTD, NTD,
    b. What protein is the HBD part of (DnaB or DnaG)?
    c. The paper mentions a technique that has been used to observe the hexameric structure of DnaB. What is this technique? Look it up and describe how it works in a few sentences.
    d. Does the interaction with DnaG have any effect on the activity of DnaB? If yes, what activities?
    e. Using the description that the authors give as a guide, describe the structure of the DnaB hexamer.
    f. How many HBD are bound to the NTD collar? Does this stoichiometry agree with the literature?

Structure of Hexameric DnaB Helicase and Its Complex with a Domain of DnaG Primase

Scott Bailey *et al.*

Science **318**, 459 (2007);
DOI: 10.1126/science.1147353

the 3′-protrusion and orient the synapsis of the ends (Fig. 2D). The 3′-overhangs of the opposing template strands are brought together via a number of base-pairing and stacking interactions (Fig. 2E and fig. S6) (*18*). Each PolDom monomer makes intimate contact with the 5′-P on the downstream strand, which is bound in a positively charged pocket formed by Lys^{16} and Lys^{26} (Fig. 3A), two residues absolutely conserved in NHEJ AEPs (fig. S4). Notably, the N-terminal PolDom region containing Lys^{16} is absent in AEPs from Archaea and Eukarya (fig. S4).

The *Mt*-PolDom mutant (Lys^{16} → Ala) was unable to bind to DNA and had very reduced polymerase activity (fig. S5), whereas gap filling was normal. Other interactions with DNA are indicated in figs. S4 and S6. The PolDom-DNA interactions are reminiscent of the contacts observed in the structure of the evolutionary unrelated NHEJ polymerase, Pol λ–gapped DNA complex (*18*, *19*) (Fig. 3).

The apical loop 1 (β5-β6) interacts with the 3′-protruding strand, thus constituting a potentially important element for maintaining the synapsis between two 3′-protruding DNA ends (Fig. 2, C and D). To analyze the functional importance of these interactions, we mutated loop 1 residues (83 to 85) to alanine and evaluated the DNA binding and polymerization capacity of the resulting mutant (*mut-loop*). On a gapped DNA substrate, the DNA binding potential of *mut-loop* was equivalent to that of wild-type PolDom (fig. S7). Therefore, the presence of a 5′-P appears to be enough to ensure enzyme-DNA stability in a gap, and loop 1 is dispensable when the primer terminus, the template, and the 5′-P are physically connected and not discontinuous. However, the integrity of loop 1 was critical to forming a synaptic complex of two 3′-protruding DNAs. Electrophoretic mobility shift and 3′-extension assays showed that *mut-loop* was very inefficient at forming a synaptic complex (fig. S8). An analogous loop-like structure may play a related role in eukaryotic NHEJ polymerases (*20*, *21*).

The importance of PolDom, and loop 1 in particular, in mediating DNA synapsis was further probed by fluorescence resonance energy transfer (FRET) using DNA with a 3′-overhang identical to that present in the crystal structure. The steady-state fluorescence spectra of doubly labeled 3′-protruding DNA (3′-fluorescein donor and 3′-rhodamine acceptor) with increasing amounts of wild-type *Mt*-PolDom showed a marked concentration-dependent increase in emission of the rhodamine fluorophore at 605 nm (Fig. 4) due to FRET from fluorescein. The presence of a PolDom-dependent FRET emission peak signifies a close approach of the 3′-overhang with the duplex region of another DNA, indicative of a stable protein-mediated interaction between two DNA ends. In contrast, the *mut-loop* mutant exhibited a markedly reduced FRET signal, indicating that loop 1 plays a critical role in stabilizing the synaptic complex. This conclusion is further supported by protein cross-linking studies (fig. S2).

The structure presented here establishes that NHEJ polymerases can promote the formation of end-bridging complexes, thereby directing the break alignment process (fig. S9). The limited number of contacts made between the enzyme and the 3′-protrusions suggests that PolDom, and presumably other NHEJ polymerases, allow a large degree of rotational freedom that enables the termini to search for sequence complementarities on the opposing break. This "homology" searching process acts, together with Ku, to align the break by forming presynaptic bridging structures, promoted by favorable microhomology-directed base pairing, that nucleate the formation of the synaptic complex (fig. S9). Thus, final end synapsis, like that shown in the crystal structure, may require a certain degree of mispairing, template dislocation, or realignment facilitated by base flipping, and the eventual formation of hairpin structures at the terminal ends. The hairpin-like structures observed—located in a large, solvent-accessible channel within the PolDom complex—could conceivably accommodate the small 3′-exonuclease domain of LigD (NucDom) (*6*, *15*), facilitating the controlled resectioning of the ends. This may possibly explain the preference of NucDom for recessed 3′-ends (*6*, *15*) and suggests that the nuclease resection process may be regulated by the conformation of the ends within the synaptic complex.

References and Notes

1. L. Krejci, L. Chen, S. Van Komen, P. Sung, A. Tomkinson, *Prog. Nucleic Acid Res. Mol. Biol.* **74**, 159 (2003).
2. J. M. Daley, P. L. Palmbos, D. Wu, T. E. Wilson, *Annu. Rev. Genet.* **39**, 431 (2005).
3. G. R. Weller *et al.*, *Science* **297**, 1686 (2002).
4. R. S. Pitcher *et al.*, *DNA Repair* **6**, 1271 (2007).
5. R. S. Pitcher *et al.*, *Mol. Cell* **23**, 743 (2006).
6. M. Della *et al.*, *Science* **306**, 683 (2004).
7. R. S. Pitcher, T. E. Wilson, A. J. Doherty, *Cell Cycle* **4**, 675 (2005).
8. R. Bowater, A. J. Doherty, *PLOS Genet.* **2**, 93 (2006).
9. C. Gong, A. Martins, P. Bongiorno, M. Glickman, S. Shuman, *J. Biol. Chem.* **279**, 20594 (2004).
10. C. Gong *et al.*, *Nat. Struct. Mol. Biol.* **12**, 304 (2005).
11. R. S. Pitcher, L. M. Tonkin, A. J. Green, A. J. Doherty, *J. Mol. Biol.* **351**, 531 (2005).
12. R. S. Pitcher *et al.*, *J. Mol. Biol.* **366**, 391 (2007).
13. L. Yakovleva, S. Shuman, *J. Biol. Chem.* **281**, 25026 (2006).
14. H. Zhu *et al.*, *Proc. Natl. Acad. Sci. U.S.A.* **103**, 1711 (2006).
15. H. Zhu, S. Shuman, *J. Biol. Chem.* **281**, 13873 (2006).
16. L. M. Iyer, E. V. Koonin, D. D. Leipe, L. Aravind, *Nucleic Acids Res.* **33**, 3875 (2005).
17. S. H. Lao-Sirieix, L. Pellegrini, S. D. Bell, *Trends Genet.* **21**, 568 (2005).
18. See supporting material on *Science* Online.
19. M. Garcia-Diaz *et al.*, *Cell* **124**, 331 (2006).
20. S. A. Nick McElhinny *et al.*, *Mol. Cell* **19**, 357 (2005).
21. R. Juárez, J. F. Ruiz, S. Nick McElhinny, D. A. Ramsden, L. Blanco, *Nucleic Acids Res.* **34**, 4572 (2006).
22. Abbreviations for amino acid residues: F, Phe; H, His; K, Lys; N, Asn; P, Pro; R, Arg; S, Ser; W, Trp.

23. We thank T. Brown, A. Lebedev, M. Osbourne, and D. Thompson for technical advice and support; T. Wilson for valuable comments on the manuscript; and the European Synchrotron Radiation Facility for provision of synchrotron radiation facilities. Work in A.J.D.'s laboratory is supported by grants from the UK Biotechnology and Biological Sciences Research Council, Cancer Research UK, the Association for International Cancer Research, and the Royal Society. Work in L.B.'s laboratory was supported by Ministerio de Ciencia y Tecnología grant BMC 2003-00186, Consolider CSD2007-00015, and an institutional grant to Centro de Biología Molecular Severo Ochoa from Fundación Ramón Areces. A.J.P. is a recipient of a fellowship from the Spanish Ministry of Science and Technology.

Supporting Online Material

www.sciencemag.org/cgi/content/full/318/5849/456/DC1
Materials and Methods
SOM Text
Figs. S1 to S9
Table S1
References

15 May 2007; accepted 14 September 2007
10.1126/science.1145112

Structure of Hexameric DnaB Helicase and Its Complex with a Domain of DnaG Primase

Scott Bailey,[1] William K. Eliason,[1] Thomas A. Steitz[1,2]*

The complex between the DnaB helicase and the DnaG primase unwinds duplex DNA at the eubacterial replication fork and synthesizes the Okazaki RNA primers. The crystal structures of hexameric DnaB and its complex with the helicase binding domain (HBD) of DnaG reveal that within the hexamer the two domains of DnaB pack with strikingly different symmetries to form a distinct two-layered ring structure. Each of three bound HBDs stabilizes the DnaB hexamer in a conformation that may increase its processivity. Three positive, conserved electrostatic patches on the N-terminal domain of DnaB may also serve as a binding site for DNA and thereby guide the DNA to a DnaG active site.

Most DNA polymerases, unlike RNA polymerases, are unable to unwind duplex DNA and require a primed single-stranded DNA (ssDNA) substrate to initiate DNA synthesis. In eubacterial cells, these functions are performed by a complex of the DnaB helicase and the DnaG primase (*1*). DnaB unwinds the duplex DNA fueled by the hydrolysis of nucleoside triphosphate (NTP) (*2*), whereas DnaG uses the newly formed

ssDNA as a template for the de novo synthesis of RNA primers (*1*). DnaB oligomerizes into a homo-hexameric ring that has been observed by electron microscopy (EM) to form either six-fold or three-fold symmetry states (*3*, *4*). The DnaB ring is thought to unwind DNA at the replication fork by translocating along and encircling the 5′ lagging strand, while the 3′ leading strand is occluded (*5*, *6*). The crystal structure of a monomer of DnaB has revealed that the helicase is composed of two domains separated by a flexible linker (*7*). The C-terminal domain (CTD) forms a RecA-like fold that contains the NTP and DNA binding sites, whereas the N-terminal domain (NTD) is composed of a helical bundle terminated by an extended helical hairpin (*7*). Although the NTD is required for helicase activity (*8*–*10*) and may define the direction of movement of the helicase on DNA (*10*), its precise function in DNA unwinding is not clear.

The interaction between DnaB and DnaG stimulates both of their activities. DnaG increases both the NTPase and the helicase activities of DnaB (*9*), and DnaB both increases and modulates the synthesis of RNA primers by DnaG (*1*). DnaG consists of three domains, an N-terminal zinc-binding domain (ZBD), an RNA polymerase domain (RPD), and a C-terminal HBD. The HBD of DnaG, whose ternary structure consists of a helical bundle (the C1 subdomain) terminated by a helical hairpin (the C2 subdomain), is sufficient to both bind to and stimulate the activities of DnaB (*9*, *11*). The tertiary structure of the HBD is highly similar to the fold of the NTD of DnaB (7, *12*, *13*). The stability of the interaction between DnaB and DnaG varies substantially among species. In *Escherichia Coli*, the interaction is relatively weak and can only be detected by sensitive techniques (*13*–*15*), whereas DnaB and DnaG from *Bacillus stearothermophilus* (*Bst*) form a tight interaction that persists when the complex is run over a gel filtration column (*9*). Despite these differences in the stability of their complexes, the biochemical behavior of DnaB and DnaG from *E. coli* and *Bst* are similar (*16*).

We have obtained two crystal structures of unliganded hexameric *Bst* DnaB (crystal forms B1 and B2) and two crystal structures of DnaB in complex with the HBD of DnaG (forms BH1 and BH2). These four crystal forms diffract x-rays to between 5.0 and 2.9 Å resolution (Table 1). Experimental phases were determined separately for each crystal form, either by the single-wavelength anomalous diffraction method using selenomethionine-substituted protein or by heavy-atom derivative methods using crystals that had been soaked in solutions containing mercury chloride (*17*). Phasing of the diffraction from each crystal form and the resulting electron density maps (Fig. 1A) were substantially improved by cross-crystal symmetry averaging among all four crystal forms (*17*). Data collection and refinement statistics for each crystal form are in Table 1. The structures of DnaB presented here differ only in the relative orientation of their CTDs. Therefore, unless otherwise stated, discussion will focus on the 2.9 Å resolution structure of DnaB complexed with HBD (form BH1), which has been refined to a free R-factor of 29.8%.

The two domains of the DnaB hexamers form a distinct double-layered ring structure in which the NTDs (residues 1 to 152) pack into a rigid triangular collar seated on top of a more loosely packed ring of CTDs (residues 186 to 454) (Fig. 1, B and C). Adjacent NTDs adopt one of two conformations that place their helical hairpins (residues 102 to 151) either on top of a neighboring CTD or on top of their own CTD (Fig. 1, C and D). These two conformations result in the six NTDs forming a trimer of head-to-head dimers related by two-fold symmetry in which three of the alternately oriented NTDs face the central channel of the ring (Fig. 1C). This trimer-of-dimers is stabilized by the hydrophobic interface that buries 2300 Å^2

Table 1. Data Collection and Refinement Statistics

Crystal Form	B1	B2	BH1	BH2
Spacegroup	$P2_12_12$	R32	P321	$P3_121$
Unit cell a,b,c (Å)	371, 110, 113	200, 200, 195	229, 229, 193	230, 230, 193
Resolution (Å)	50 – 3.7	50 – 5.0	50 – 2.9	50 – 4.0
Rmerge (%)*	8.1 (59.0)	5.8 (53.3)	7.0 (>100)	10.3 (50.3)
Completeness (%)*	97.3 (86.6)	95.8 (74.5)	99.8 (99.9)	99.9 (100.0)
I/σI*	15.0 (1.4)	35.9 (3.5)	22.3 (1.9)	19.6 (3.6)
Rwork*	30.8 (36.0)	39.4 (48.3)	25.9 (32.4)	32.0 (34.0)
Rfree*	32.3 (35.8)	39.7 (49.1)	29.7 (40.0)	34.4 (38.4)
RMSD† bond (Å)/angle (°)	0.009/1.416	–/–	0.009/1.389	0.010/1.659

*Values in parentheses correspond to the last resolution shell. †Root mean square deviation.

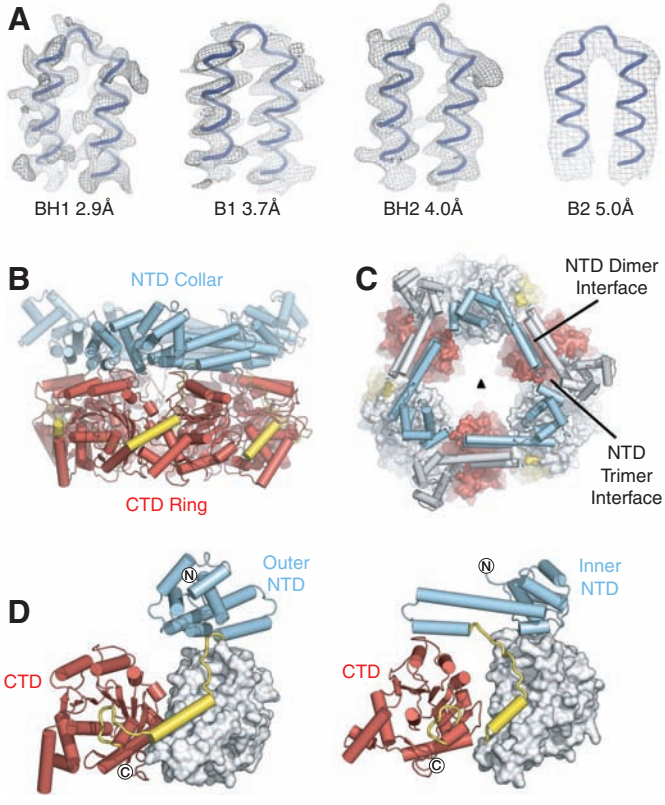

Fig. 1. Architecture of the DnaB hexamer. (**A**) Experimentally phased and cross-crystal averaged electron density maps of the four DnaB crystal forms. Shown at the foot of each map is the high-resolution limit at which each map was calculated. (**B**) "Side" view, orthogonal to the ring axis, of a ribbon representation of the DnaB hexamer. The NTD, CTD, and linker region are colored blue, red, and yellow respectively. (**C**) "Top" view, looking down the ring axis, of the DnaB hexamer. The CTDs are shown in a surface representation; the NTDs are shown as ribbons. Those subunits whose NTDs lie on the inner surface of the ring are colored as in (B), and those on the outer surface of the ring are colored white. (**D**) "Side" view of the two distinct conformations of the DnaB subunits within the hexamer, colored as in (B). Adjacent CTDs interacting with the linker region are shown as white surface representations.

[1]Department of Molecular Biophysics and Biochemistry and Howard Hughes Medical Institute, Yale University, New Haven, CT 06520, USA. [2]Department of Chemistry, Yale University, New Haven, CT 06520, USA.

*To whom correspondence should be addressed. E-mail: eatherton@csb.yale.edu

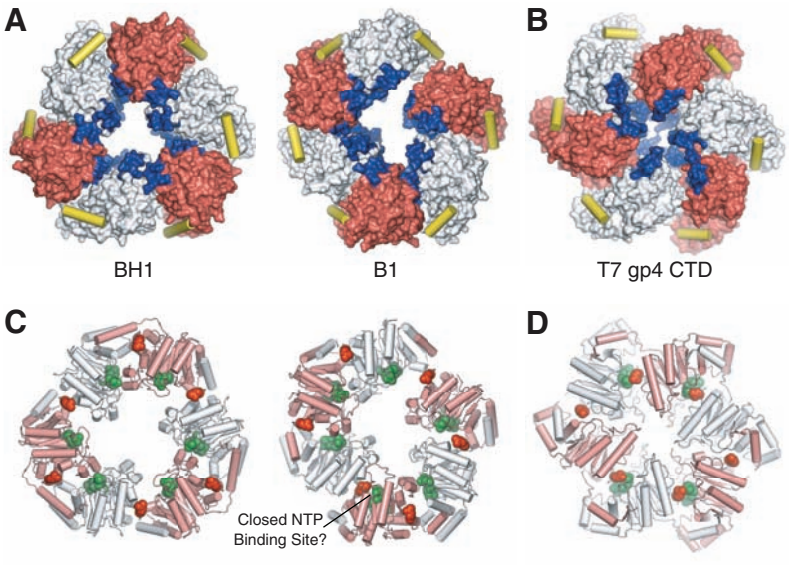

Fig. 2. Structure of the CTD ring. (**A**) Surface representation of the CTD rings of crystal forms BH1 (left) and B1 (right). Alternate subunits are colored white and red. The predicted DNA binding loops are colored blue, and the linker helices are shown as yellow cylinders. (**B**) The structure of the T7 gp4 helicase domain (*23*), displayed as in panel (A). (**C**) Ribbon representations of the CTD rings of crystal forms BH1 (left) and B1 (right). Alternate subunits are colored white and pink. NTP modeled at the six potential NTP binding sites of DnaB (22) are shown as green spheres; the Arginine fingers (Arg^{420}) are displayed as red spheres. (**D**) The structure of the T7 gp4 hexamer with four NTD binding sites occupied, displayed as in (C).

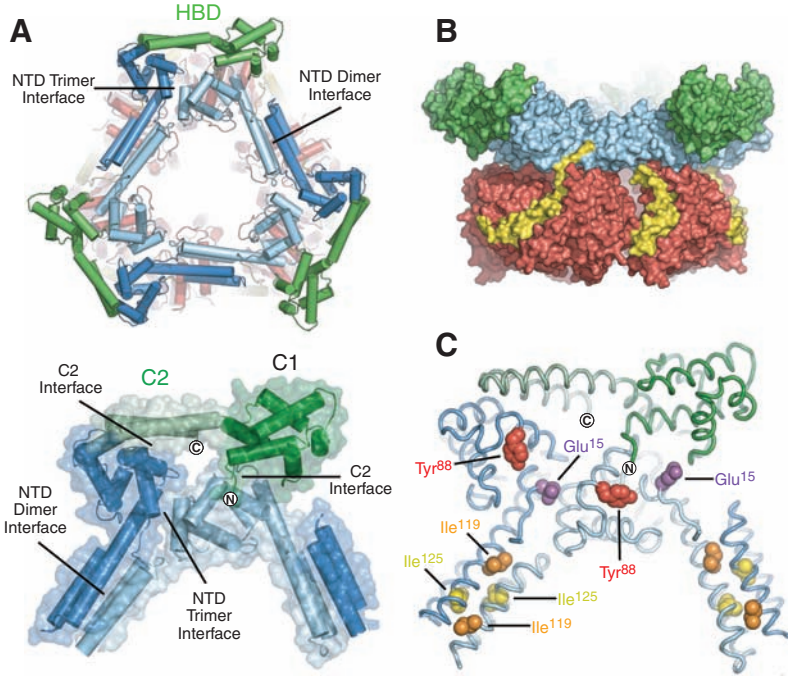

Fig. 3. Structure of the complex between DnaB and HBD. (**A**) (Top) "Top" view of a ribbon representation of the complex showing the three HBDs (green) bound at the periphery of the NTD collar (light blue and blue). The CTD and linker region are colored red and yellow, respectively. (Bottom) The interface between DnaB and HBD shown as ribbons with a transparent surface. (**B**) "Side" view of a surface representation of the complex revealing no interaction between the HBDs (green) and the DnaB CTD (red) or linker region (yellow). (**C**) Backbone trace of the HBD DnaB interface, residues known to modulate the interaction between DnaB and DnaG, are shown as colored spheres.

within the dimers and by the hydrophobic interface between dimers that buries 1050 $Å^2$ total surface area. Formation of the NTD collar appears to be highly cooperative, requiring the presence of the CTD, because truncated protein containing the NTD alone forms either monomers or dimers (*9*). Despite differences in crystal packing interactions of the NTDs, the structures of the NTD collar are similar in all four crystal forms (fig. S1).

Comparison of the structures of the four DnaB hexamers shows that their CTDs adopt a variety of different orientations around the ring but still bind the linker helix (residues 162 to 178) of the adjacent subunit at the periphery of the hexamer and orient their proposed DNA binding loops (*18*) toward the central channel (Fig. 2A and fig. S2). With the exception of the B1 structure, in which the CTDs form a distinctly irregular ring with no rotational symmetry, all of the CTD rings exhibit either exact or approximate three-fold symmetry (Fig. 2A and fig. S2). The hexameric rings of CTDs are held together primarily by their interactions within the linker region and not by interactions between adjacent CTDs. The interaction surface between adjacent CTDs in the four crystal structures ranges from little or none to 1100 $Å^2$ of total surface area, whereas the interface between each subunit and the linker region bury 2250 $Å^2$ of surface area (Fig. 1D). In addition to these interactions, the CTD ring appears to be additionally stabilized by the interactions between the NTDs, because mutants lacking the NTD have reduced hexamer stability (9, *19*).

The DnaB hexamer assembly has an outer diameter of 115 Å and a height of 75 Å. The diameter of the central channel through the NTD collar is ~50 Å, whereas the different orientations of the CTD rings result in channel diameters that vary between ~25 Å and ~50 Å in the four crystal structures. Thus, in the absence of its substrates, the diameter of the central channel of DnaB is wide enough to accommodate duplex DNA. Currently the crystal structure of the papillomavirus E1 helicase complexed with ssDNA and ADP (*20*) is the only high-resolution structure of a hexameric helicase bound to DNA. Because the E1 helicase uses different regions of its RecA-like domains for hexamer formation and DNA binding (*7*), the structure of DnaB bound to ssDNA must differ. However, it has been suggested that the spiral conformation of the bound ssDNA observed in E1 helicase structure may be common to all hexameric helicases (*20*). Fluorescence titration experiments have shown that DnaB binds ssDNA with a site size of ~20 bases (*21*). If the average distance between bases is 3.5 Å in the complex with DnaB, as was observed for E1 helicase (*20*), the DNA would extend ~70 Å, consistent with the 75 Å height of hexameric DnaB structures. The shape and dimensions of the crystal structures of DnaB are inconsistent with the shape and dimensions of the three-dimensional (3D) EM reconstructions of *E. coli*

DnaB (*3*) and G40P (*4*) (fig. S3); however, they are consistent with the 2D EM projections used to generate the 3D reconstructions. Therefore, it seems likely that the differences between the crystal and 3D EM data could be due to distortions generated by the negative staining process or to the methodological difficulties of generating 3D reconstructions of molecules as flexible as DnaB (discussed further in supporting online text).

The T7 gp4 protein of phage T7 contains two domains, one responsible for the helicase activity and the other for the primase activity, which are necessary for the replication of the T7 phage (*22*). Although the CTD of gp4 is homologous to the CTD of DnaB, gp4 lacks a domain equivalent to the DnaB NTD (*7*, *23*). Instead, two domains related to the ZPD and RPD of DnaG are fused to the N terminus of the protein. The crystal structure of the hexameric CTD of gp4 bound to a nonhydrolysable NTP analog (*18*) shows that the NTP binding pockets are formed between adjacent CTDs (Fig. 2, B and D). The majority of each pocket is formed by one CTD, whereas the adjacent CTD provides an arginine residue, the arginine finger, whose guanadinium group contacts the γ-phosphate of the bound NTP. The arginine finger is believed to stimulate NTP hydrolysis and to help modulate the relative orientation of the CTDs in response to NTP hydrolysis (*18*, *24*).

Comparison of the structures of DnaB and the gp4 helicase shows that the oligomerization of the two proteins is facilitated by a similar linker helix (Fig. 2), but the contacts between the adjacent CTDs of gp4 are much more extensive than those seen in DnaB. These more extensive contacts are generated by a rotation of the gp4 CTDs, both toward and about the plane of the hexamer ring, and result in a tighter gp4 hexamer that contains a central channel only wide enough to accommodate ssDNA (Fig. 2). The larger diameter of the central channels observed in the DnaB structures is probably due to the absence of bound NTP (supporting online text), because a more extended conformation of DnaB has been observed by EM in the absence of nucleotide (*3*). In addition, as a result of the orientations of the DnaB CTDs, most of the NTP binding sites are not near an arginine finger (Fig. 2C). Only the B1 structure has one pair of adjacent CTDs that position an arginine finger close enough to interact with the γ-phosphate of a bound NTP (Fig. 2C). This interface maybe representative of a nucleotide-bound state of DnaB. However, homology between the CTDs of DnaB and gp4 and the fact that superimposing the structure of the DnaB CTD onto the six CTDs of the nucleotide-bound gp4 structure produces a model with no steric clashes (*7*) suggest that the complex with nucleotide will orient the CTDs of DnaB to form a central channel that is only wide enough to accommodate ssDNA. The ability of DnaB to modulate the diameter of its central channel is, however, consistent with the observation that DnaB can translocate on ssDNA even when a complementary strand is present within the central channel (*25*).

Three molecules of the HBD are bound to the NTD collar of the DnaB hexamer in the structures of the complex (Fig. 3A). This stoichiometry agrees with analytical ultracentrifugation and gel filtration studies of the complex between *Bst* DnaB and DnaG, which show that between two and three molecules of DnaG bind to each DnaB hexamer (*9*). This number is also consistent with fluorescence anisotropy and cross-linking experiments conducted using the complex of *E. coli* DnaB and DnaG (*15*). The bound HBDs do not interact with either the CTD or the linker region of DnaB (Fig. 3B); consequently, there is no correlation between HBD binding and the position of the CTDs or the diameter of the CTD rings in the four structures presented here. The C2 subdomains of the HBD pack against the NTDs that form the outer surface of the ring while the C1 subdomains interact with the NTDs that form the inner surface of the ring (Fig. 3). Both interfaces are formed by a mixture of hydrophobic and polar contacts and each burry ~1200 Å^2 of total surface area (fig. S4). The C-terminal helix of the HBD (residues 577 to 595 in *Bst*) forms the majority of the interface with the C2 subdomain which is consistent with mutagenesis studies of *E. coli* DnaB (*11*). Overall, the interface with the C1 subdomain is less tightly packed than that with the C2 subdomain, perhaps explaining why the isolated C2 subdomains can form a gel filterable complex with DnaB, whereas the isolated C1 subdomain cannot (*12*). The C2 subdomain of *E. coli* DnaB is smaller than that of Bst DnaB, which also may explain why Bst DnaB and DnaG form a more stable complex than their *E. coli* counterparts (for more details, see supporting online text). The binding of one molecule of HBD to two NTD dimers effectively fixes the three-fold arrangement of the NTD collar (Fig. 3A), consistent with previous atomic force microscopy results (*26*).

Mutation of residues Tyr^{88}, Ile^{119}, or Ile^{125} in *Bst* DnaB (*16*, *26*) and of the equivalent residues in *E. coli* (*27*–*29*) and *Salmonella typhimurium* (*30*) inhibits the formation of a complex between DnaB and DnaG. Because Tyr^{88} lies near the interface with the HBD but does not directly contact it (Fig. 3C), this mutation presumably disrupts the tertiary structure of the NTD helical bundle. Residues Ile^{119} and Ile^{125} are buried from solvent at the NTD dimer interface (Fig. 3C), which suggests that their mutation would disrupt dimerization of the NTD. Hence, inhibition of DnaG binding by these mutants would appear to result from the destabilization of the trimer-of-dimers arrangement of the DnaB NTDs. Indeed, it has already been suggested that these mutant helicases may have altered NTD positions (*27*). Mutation of Glu^{15} in *Bst* DnaB has no effect on its binding to DnaG but does modulate the length of the primers synthesized by DnaG (16). The equivalent mutation in *E. coli* and *S. typhimurium* inhibits the binding of DnaG (*27*, *30*). Glu^{15} lies both at the C1 subdomain binding site and at the NTD trimer interface (Fig. 3C), consistent with its having a role in the formation of a DnaG complex. How this residue modulates primer synthesis in the complex of *Bst* DnaB and DnaG is currently not clear.

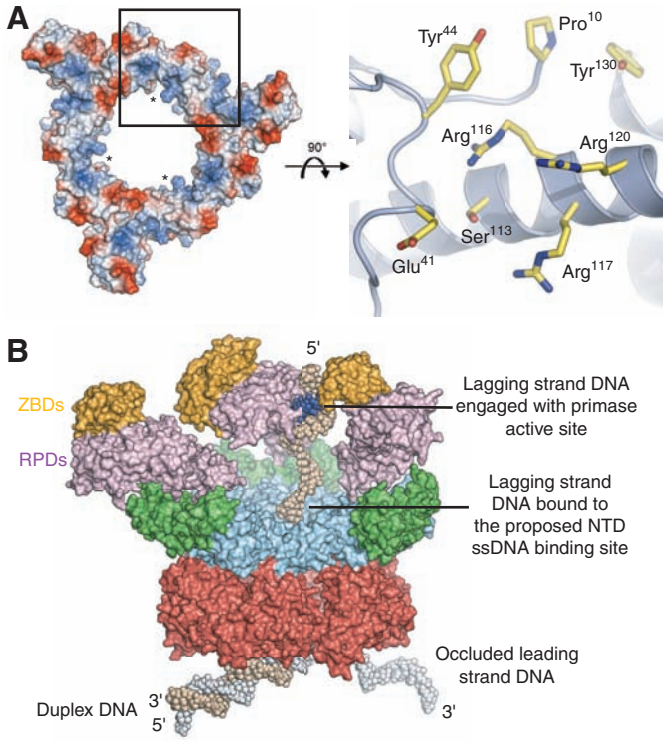

Fig. 4. DNA interactions. (**A**) (Left) "Top" view of a surface representation of the NTD collar colored blue for positive and red for negative electrostatic potentials. An asterisk highlights the proposed ssDNA binding sites. (Right) A detailed "side" view of the proposed ssDNA binding site boxed in (A). (**B**) Speculative model of DnaB complexed with DnaG and replication fork DNA. The proteins are shown in a surface representation (DnaB NTD, light blue; DnaB CTD, red; DnaG HBD, green; DnaG RPD, pink; and DnaG ZBD, orange). The modeled DNA is shown as white- and wheat-colored spheres; the RNA primer is shown in dark blue.

The binding of DnaG to DnaB stimulates the activities of DnaB (*1*) and stabilizes the three-fold conformation of the DnaB NTDs. This suggests that the three-fold symmetric state represents an activated form of DnaB; therefore, it seems doubtful that the DNA translocation mechanism of DnaB involves transitions between six- and three-fold symmetries. Both DnaB and the T7 gp4 proteins require a stable hexamer for NTPase and helicase activity (*9*, *18*). Therefore, the DnaG-mediated stimulation of the activities of DnaB could also result from the increased stability of the hexamer produced by the binding of DnaG, which is consistent with the observation that although the isolated C2 subdomain of the HBD can bind DnaB, both subdomains of the HBD are required for the stimulation of the activities of DnaB (16). Although the presence of DnaG at the replication fork in *E. coli* has been shown to be distributive (*31*), the binding of only one molecule of DnaG to DnaB would be sufficient to stabilize the three-fold conformation of DnaB. The closed circular structure of the NTD collar could also contribute to the stimulation of the helicase activity by keeping the two ssDNA strands topologically separated during unwinding. In addition the topological linking of DnaB to the DNA also would ensure that the two molecules could not easily disengage, thus increasing the processivity of the reaction. Kinetic analysis has shown that isolated DnaB is only a moderately processive enzyme, and it is assumed that it gains the processivity needed to replicate the genome from other components of the replication fork (*32*). A similar processivity role has also been suggested for the unrelated NTD of the papillomavirus E1 helicase (*20*).

The NTD collar may also provide an additional binding site for ssDNA. The interior surface of the NTD collar exhibits three distinct sites of positive electrostatic potential separated by regions of negative electrostatic potential (Fig. 4A). These positive sites are consistent with their binding DNA, contain residues that are conserved across DnaB species, and are well positioned for binding the ssDNA as it emanates from the CTD ring (Fig. 4). Nuclease protection and fluorescence energy transfer studies have also suggested the presence of a second ssDNA binding site at the N terminus of DnaB (*33*).

It is now possible to construct a model of the complex between DnaB and DnaG that illuminates how they cooperatively work together and stimulate each other's activities. The N terminus of each HBD is situated adjacent to the central channel of DnaB (Fig. 3), thereby positioning the N-terminal ZBD and RPD of full-length DnaG directly above the central channel (Fig. 4B). Thus, the structure of the RPD-ZBD fragment (*34*) can be positioned relative to the HBD in a manner that orients the primase active site with the proposed N-terminal ssDNA binding site of DnaB and is consistent with the structure of the truncated T7 gp4 helicase-primase heptamer (*21*). The structure of the complex between DnaB and HBD, and our modeling of the complex between the full-length proteins, is consistent with the possibility that DnaB stimulates the activity of DnaG by increasing the local concentration of the ssDNA substrate and by ensuring that multiple DnaG subunits are in close proximity to each other (*35*) (Fig. 4B). The latter is important because the RPD and ZBD function have been shown to function in trans, with each domain provided by a separate subunit (*35*).

References and Notes

1. J. E. Corn, J. M. Berger, *Nucleic Acids Res.* **34**, 4082 (2006).
2. J. H. LeBowitz, R. McMacken, *J. Biol. Chem.* **261**, 4738 (1986).
3. S. Yang *et al.*, *J. Mol. Biol.* **321**, 839 (2002).
4. R. Nunez-Ramirez *et al.*, *J. Mol. Biol.* **357**, 1063 (2006).
5. M. J. Jezewska, S. Rajendran, D. Bujalowski, W. Bujalowski, *J. Biol. Chem.* **273**, 10515 (1998).
6. D. L. Kaplan, *J. Mol. Biol.* **301**, 285 (2000).
7. S. Bailey, W. K. Eliason, T. A. Steitz, *Nucleic Acids Res.* **35**, 4728 (2007).
8. N. Nakayama, N. Arai, Y. Kaziro, K. Arai, *J. Biol. Chem.* **259**, 88 (1984).
9. L. E. Bird, H. Pan, P. Soultanas, D. B. Wigley, *Biochemistry* **39**, 171 (2000).
10. P. Mesa, J. C. Alonso, S. Ayora, *J. Mol. Biol.* **357**, 1077 (2006).
11. K. Tougu, K. J. Marians, *J. Biol. Chem.* **271**, 21391 (1996).
12. K. Syson, J. Thirlway, A. M. Hounslow, P. Soultanas, J. P. Waltho, *Structure* **13**, 609 (2005).
13. A. J. Oakley *et al.*, *J. Biol. Chem.* **280**, 11495 (2005).
14. Y. B. Lu, S. Bhattacharyya, M. A. Griep, *Proc. Natl. Acad. Sci. U.S.A.* **93**, 12902 (1996).
15. A. V. Mitkova, S. M. Khopde, S. B. Biswas, *J. Biol. Chem.* **278**, 52253 (2003).
16. J. Thirlway, P. Soultanas, *J. Bacteriol.* **188**, 1534 (2006).
17. Materials and methods are available as supporting material on *Science* Online.
18. M. R. Singleton, M. R. Sawaya, T. Ellenberger, D. B. Wigley, *Cell* **101**, 589 (2000).
19. S. B. Biswas, P. H. Chen, E. E. Biswas, *Biochemistry* **33**, 11307 (1994).
20. E. J. Enemark, L. Joshua-Tor, *Nature* **422**, 270 (2006).
21. W. Bujalowski, M. J. Jezewska, *Biochemistry* **34**, 8513 (1995).
22. E. A. Toth, Y. Li, M. R. Sawaya, Y. Cheng, T. Ellenberger, *Mol. Cell* **12**, 1113 (2003).
23. M. R. Sawaya, S. Guo, S. Tabor, C. C. Richardson, T. Ellenberger, *Cell* **99**, 167 (1999).
24. D. J. Crampton, S. Guo, D. E. Johnson, C. C. Richardson, *Proc. Natl. Acad. Sci. U.S.A.* **101**, 4373 (2004).
25. D. L. Kaplan, *J. Mol. Biol.* **301**, 285 (2000).
26. J. Thirlway *et al.*, *Nucleic Acids Res.* **32**, 2977 (2004).
27. L. Stordal, R. Maurer, *J. Bacteriol.* **178**, 4620 (1996).
28. P. Chang, K. J. Marians, *J. Biol. Chem.* **275**, 26187 (2000).
29. Y. B. Lu, P. V. A. L. Ratnakar, B. K. Mohanty, D. Bastia, *Proc. Natl. Acad. Sci. U.S.A.* **93**, 12902 (1996).
30. R. Maurer, A. Wong, *J. Bacteriol.* **170**, 3682 (1988).
31. C. A. Wu, E. L. Zechner, K. J. Marians, *J. Biol. Chem.* **267**, 4030 (1992).
32. R. Galletto, M. J. Jezewska, W. Bujalowski, *J. Mol. Biol.* **343**, 83 (2004).
33. M. J. Jezewska, S. Rajendran, W. Bujalowski, *J. Biol. Chem.* **273**, 9058 (1998).
34. J. E. Corn, P. J. Pease, G. L. Hura, J. M. Berger, *Mol. Cell* **20**, 391 (2005).
35. S. J. Lee, C. C. Richardson, *Proc. Natl. Acad. Sci. U.S.A.* **99**, 12703 (2002).

36. This research was supported by NIH grant GM57510 to T.A.S. We thank P. Soultanas for the expression plasmids. Coordinates and structure factors of crystal forms BH1, BH2, B1, and B2 have been deposited under accession codes 2R6A, 2R6C, 2R6D, and 2R6E, respectively.

Supporting Online Material

www.sciencemag.org/cgi/content/full/318/5849/459/DC1
Materials and Methods
SOM Text
Figs. S1 to S7
Tables S1 and S2
References

3 July 2007; accepted 11 September 2007
10.1126/science.1147353

Network Analysis of Oncogenic Ras Activation in Cancer

Edward C. Stites,[1,2,3] Paul C. Trampont,[1] Zhong Ma,[1] Kodi S. Ravichandran[1]*

To investigate the unregulated Ras activation associated with cancer, we developed and validated a mathematical model of Ras signaling. The model-based predictions and associated experiments help explain why only one of two classes of activating Ras point mutations with in vitro transformation potential is commonly found in cancers. Model-based analysis of these mutants uncovered a systems-level process that contributes to total Ras activation in cells. This predicted behavior was supported by experimental observations. We also used the model to identify a strategy in which a drug could cause stronger inhibition on the cancerous Ras network than on the wild-type network. This system-level analysis of the oncogenic Ras network provides new insights and potential therapeutic strategies.

Ras is a small guanosine triphosphatase (GTPase) that binds the guanine nucleotides guanosine triphosphate (GTP) and guanosine diphosphate (GDP) (*1*, *2*). Ras bound to GTP (Ras_{GTP}) is the "active" form with which downstream effector proteins spe-